Phase Sensitive Control of Vibronic Guest−Host Interaction: Br_2 in Ar Matrix†

Heide Ibrahim,‡ Mónika Héjjas,‡ Mizuho Fushitani,§ and Nikolaus Schwentner*,‡

Institut für Experimentalphysik, Freie Universität Berlin, Arnimallee 14, D-14195 Berlin, Germany, and Institute for Molecular Science, Myodaiji, Okazaki, 444-8585, Japan

Received: January 12, 2009

Vibronic progressions are programmed into a pulse shaper which converts them via the inherent Fourier transformation into a train of femtosecond pulses in time domain for chromophore excitation. Double pulse results agree with phase-sensitive wave packet superposition from a Michelson interferometer which delivers coherence times with high reliability. Spectral resolution of 1 nm and a spacing of around 4 nm within the 20 nm envelope centered at 590 nm delivers a train of seven phase-controlled 40 fs subpulses separated by 250 fs. Combs adjusted to the zero phonon lines (ZPL) and phonon sidebands (PSB) of the B state vibronic progression are reproduced in the chromophore for a coherent subpulse accumulation. B state ZPL wave packet dynamics dominates in pump−probe spectra due to its coherence despite an overwhelming but incoherent A state contribution in absorption. PSB comb accumulation is also phase sensitive and demonstrates coherence within several 100 matrix degrees of freedom in the vicinity.

1. Introduction

Coherent control scenarios are extensively explored in relation to quantum computing and manipulation of photochemical reactions.[1,2] Their application requires the extension from a few to many degrees of freedom, which goes along with an increasing tendency to decoherence. Decoherence times for electronic transitions on the order of 100 fs are expected for chromophores in the condensed phase which are the topic of this contribution. These short times are comparable to typical periods of the vibrational degrees of freedom, and they represent a severe challenge for the application of coherent control schemes. As a standard situation it can be anticipated that some special degrees may remain coherent for some periods. They can be burried in an overwhelming background of contributions which undergo quick decoherence. Indeed, optimal control experiments delivered successful optimization in systems with rather featureless spectra originating from congestion and damping.[2] In addition, parametrically programmed coherent pulse trains enabled amplification of individual vibrations.[3]

Here we demonstrate that two tools, the unbalanced Michelson interferometer and the programmable shaping of a dispersed light pulse, can be combined for a systematic search and amplification of coherent traces. We employ a standard pulse shaper unit with 4f optics and a liquid crystal display (LCD) in the Fourier plane where the wavelength-resolved pulse is located between the dispersing and recombining gratings. Typically, wavelength-resolved spectra guide the search for possible coherent features, and we prove that a direct programming of such features delivers intuitive and well matching pulse trains concerning phase and amplitude distributions. Pulse properties are demanded for coherent control of multiple degrees of freedom which seem at first sight to be incompatible with the uncertainty relationship. Short pulses with a large spectral width are required to prepare dynamically propagating wave packets from a coherent superposition of several eigenstates of the mode under consideration. However, also eigenstates of other degrees of freedom will be lying in the same spectral region and become thus excited. Therefore, a spectral selection of individual modes achievable in highly wavelength resolved spectroscopy seems to be lost. Heller emphasized the intimate relation of the propagating vibrational wave packet on an electronic potential with its frequency representation, the absorption spectrum, via a Fourier transformation.[4,5] We utilize this picture of already propagating wave packets interfering with wave packets just generated in the Franck−Condon region of an electronic transition according to the time-dependent electric field. In this framework it is immediately evident that the amplitude and phase information of the exciting electric field is stored in the propagating wave packet as long as its coherence is preserved. Thus, a sequence of light pulses with a time separation tuned to the recurrence time of the wave packet in the Franck−Condon region results in a frequency-comb-like preparation of the wave packet. This intramolecular interference is operative despite the fact that the individual light pulses are shorter than the period and do not interact with each other. Tuning this frequency comb toward resonance with different modes will be the key to resolve the resolution problem. Steering in this way the coupling of an intramolecular mode with modes of a crystalline environment will be demonstrated. Here, tasks will be shared by exploiting the Michelson interferometer device in order to explore the number of coherent recurrencies within the decoherence inducing environment. The pulse shaper delivers an optimal pulse sequence for comb preparation. A straightforward spectral programming into the wavelength dispersed light pulse on the LCD delivers Fourier transformed pulse sequences with a time structure of the electric field which would be difficult to address directly in time space.

This is illustrated for an anharmonic intramolecular oscillator distorted in addition by curve crossings and the interaction with the host. The proof of principal type of experiment is carried out for Br_2 molecules embedded in an Ar crystalline matrix. Dihalogens in matrices were explored in a long standing effort to study basic properties of guest−matrix interaction and photochemistry in the condensed phase. In Gerber's group,

* Corresponding author, nikolaus.schwentner@physik.fu-berlin.de.
† Part of the "Robert Benny Gerber Festschrift".
‡ Institut für Experimentalphysik, Freie Universität Berlin.
§ Institute for Molecular Science.

10.1021/jp900287m CCC: $40.75
Published on Web 03/23/2009

molecular dynamics simulations for F_2 dissociation and the guiding of F atom motion in a rare gas matrix were carried out already in ref 6. The insight was deepened by intense collaborations within a large variety of groups in theory and experiment as documented for example in ref 7. Two major directions emerged. First, the treatment of nonradiative transitions induced by the coupling to the matrix was steadily improved from classical molecular dynamics calculations to semiclassical approaches and recently even to full quantum mechanical calculations.[8,9] Second, the Gerber group was very successful in predicting new members of the quickly growing family of rare gas compounds and simulating their key fingerprints.[10,11] Those compounds require the matrix for stabilization and as a reaction partner and represent thus benchmark solid state reactions. If the investigations presented here are successful, then they open the way to coherently control a basic photochemical reaction, i.e., the theoretically treated matrix-induced predissociation of Br_2 in Ar.[12] One may speculate that in the future the two branches merge again in the controlled production of new rare gas compounds.

Br_2 in Ar matrix was chosen for the following reasons: The X → B transition shows a long vibrational progression in the suitable spectral region of 650−500 nm.[13] A recent improved investigation clarified the vibrational assignment, the contribution of the X → A transition to excitation and fluorescence spectra and the population flow from B to A and A′ via several crossings with repulsive states.[14] The B vibrational levels in excitation are characterized by zero phonon lines (ZPL), i.e., an exclusive excitation of the Br_2 chromophore vibrations without participation of vibrations (phonons) in the surrounding lattice. The Br_2 molecule fits according to the van der Waals radii very well in a double substitutional site of the lattice. The surrounding well-ordered face-centered cubic Ar lattice inhibits rotational motions. The line width of the ZPL is small and essentially determined by the lifetime which indicates that indeed inhomogeneous broadening can be ignored. The ZPL are accompanied on the blue side by broad phonon sidebands (PSB) which represent a simultaneous excitation of a Br_2 vibration and phonon modes of the environment. The PSB are structured and represent very well the matrix phonon density of states. The structures have been reproduced recently also convincingly in multidimensional quantum calculations of the normal mode spectrum.[15] The ZPL and PSB progressions will be the key features to be addressed in the present investigation by frequency combs in the molecule initiated by pulse trains.

The small line widths of the ZPL signal long coherence. The first goal will be to separate out the ZPL coherences from the PSB part which is certainly more exposed to decoherence. The next step however will be a search for coherence in the PSB. To our surprise we find lasting coherences also in the PSB. There is in addition another challenge which connects this system with the prototypical situation mentioned in the beginning of "lost" coherence signatures in a dominant background of incoherent structureless contributios. In the chosen spectral region (around 590 nm) which is relevant for future predissociation studies the Franck−Condon factors of the X → A transition are several orders of magnitude larger than those of the X → B transition. In addition, the X → A transition lies above the A state gas phase dissociation limit. Therefore, the A state is bound only by the matrix cage and the accompanied large energy loss in the first excursion leads in the spectral range to a structureless continuum. As a consequence the B state ZPL around 590 nm are hardly recognizable in absorption on the A state background and the PSB is not discernible at all.[14] Here a key problem has to be solved: Is it possible to enhance B state coherences by pulse trains to such an extent that not only ZPL but also PSB can be manipulated with the molecular frequency comb?

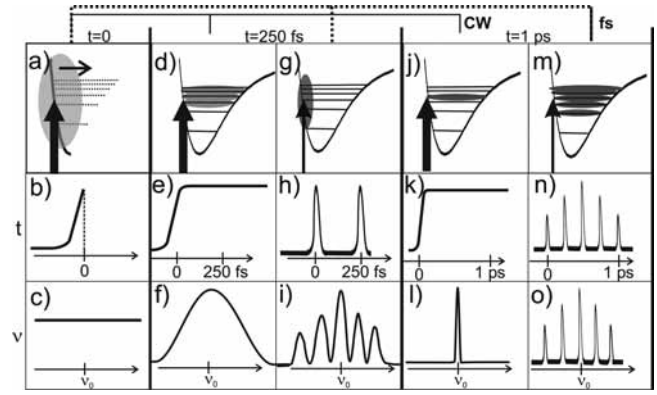

Figure 1. Wave packet scheme for autocorrelation with nanosecond excitation (CW) and cross correlation (fs) with a pulse train of ultrashort pulses at three different times ($t = 0$, 250 fs, and 1 ps) in the first row for an average round trip time in the potential of 250 fs. The second row displays schematically the time evolution of light intensity with changing scale as given by the numbers and the third row the corresponding line shape in frequency domain on a fixed scale. Thereby each column describes the same situation, respectively.

2. Pulse Structure and Experiment

2.1. Pulse Structure. The formal equivalence of the dynamical description by a propagating vibrational wave packet according to Heller's approach with the absorption spectrum in frequency space and the connection via Fourier transformation is well-known. It has been worked out in detail with emphasis on the time representation for example in ref 16. It is relevant for an appropriate application of the two experimental tools and therefore illustrated in Figure 1. The top row shows a schematic anharmonic potential with vibrational eigenstates and the shaded part stands for the spatial and energetic extension of the population. The second and third row show the excitation pulse in time and frequency. The label "CW" illustrates the typical case of frequency resolved absorption spectroscopy while "fs" represents time-resolved wave packet interferometry, here for a vibrational round trip time of 250 fs. The first column with $t = 0$ corresponds to a nearly instantaneous turn-on of both light sources with a rising flank on the order of the electric field frequency, i.e., a few femtoseconds (Figure 1b) and equivalently to the short time an essential white light frequency spectrum (Figure 1c). A wave packet is created in the Franck−Condon region, here on the inner limb (Figure 1a) on the repulsive part of the potential. It extends continuously over a wide range in energy but remains located in the Franck−Condon region due to the short propagation time. The bounding right-hand part of the potential did not yet come into play and eigenstates are not yet relevant; however, the wave packet expands and travels in this direction. In the continuous wave (CW) case the light stayed on continuously for 250 fs in Figure 1e and the central frequency υ_0 is well-defined (Figure 1f). The propagating wave packet interacts continuously in time with the newly created parts and will start to center on few eigenstates (Figure 1d) which provide constructive interference conditions. In the femtosecond case the first pulse has terminated quickly, and the created spatially tight wave packet has passed the outer turning point and arrives once more in the Franck−Condon region (Figure 1g) where it interferes with the wave packet just being generated by the

second pulse of Figure 1h. This is the tutorial wave packet interferometric situation in the Michelson case. A rather long delay (here 250 fs) has to be provided in order that the two wave packets match in the Franck−Condon region. Nevertheless, a subfemtosecond fine-tuning determines whether the phase of the electric fields prepares a wave packet which matches constructively with the previous one and enlarges it or if both cancel each other. Both light pulses do not see each other but a frequency analysis in a monochromator where both pulses are stretched or analogously the interaction in the memory of the molecular wave function delivers a sinusoidal comb within the envelope as displayed in Figure 1i. In frequency space it means that the comb matches with the eigenstates (Figure 1g) in the constructive case or lies between them in the destructive case. After 1 ps in the CW case the continuous pulse in time (Figure 1k) produces a spectrally sharp line around υ_0 (Figure 1l), and if υ_0 is resonant with the transition energy, a single eigenstate will be prepared (Figure 1j). In the fs regime we can now apply five pulses equally spaced in time, separated by 250 fs (Figure 1n). In the molecular wave function they correspond to a spectral comb with once more the vibrational spacing like in Figure 1o. It lies on the eigenstates for constructive phases of each of them or all of them cancel in the destructive case. The spectral width of each tooth sharpens with coherent addition of further pulses (Figure 1o) in mathematical analogy to the spectral resolution of a grating which improves with the number of contributing lines. The spectral envelope over all teeth is determined like in Figure 1i by the pulse length of the individual pulses. Thus, application of a phase stable pulse train to a still coherent molecular excitation allows to spectrally select with resolution improving with the number of pulses and to prepare in addition a spatially narrow wave packet by a coherent superposition of eigenstates according to the shortness of the subpulses.

The single round trip time corresponding to a harmonic oscillator with equal vibrational spacing does not hold for the real molecular system. Therefore, more sophisticated pulse sequences concerning amplitude and phase have to be employed in reality. Figure 1o illustrates that a correct spectral definition of the pulses with respect to eigenstate energies leads automatically to the required sophisticated timing properties. Usually we have the spectral information better at hand and therefore a spectral programming of the LCD in Figure 2 favored by us is presumably in many cases superior to the parametric[3] or closed loop[17] programming discussed in the literature. Excitation around 590 nm of Br_2 in Ar prepares with a moderate Franck−Condon factor a wave packet in the A state in the gas phase dissociation continuum according to Figure 3 which dominates the absorption spectrum.[14] The cage effect causes recombination with strong energy loss. Fast vibrational relaxation with respect to the long radiation lifetime leads to fluorescence from A($\upsilon' = 0$) and from A′($\upsilon' = 0$) to X(υ'') with high quantum efficiency. A second wave packet is prepared in the B state with much smaller Franck−Condon factors and most of this small population funnels by predissociation again into A($\upsilon' = 0$) and A′($\upsilon' = 0$) from where it decays radiatively (Figure 3). A high-resolution CW excitation spectrum of the A′ fluorescence is shown as dark solid line in Figure 4b. It is similar to an absorption spectrum and shows the dominating A state continuum excitation with hardly discernible small spikes from the weak but well-resolved B state vibrational progression. A small fraction of B state population survives predissociation and relaxes to B($\upsilon' = 0$) from where it radiates well separated from A and A′ fluorescence. Therefore, in the B-state excitation spectrum shown gray

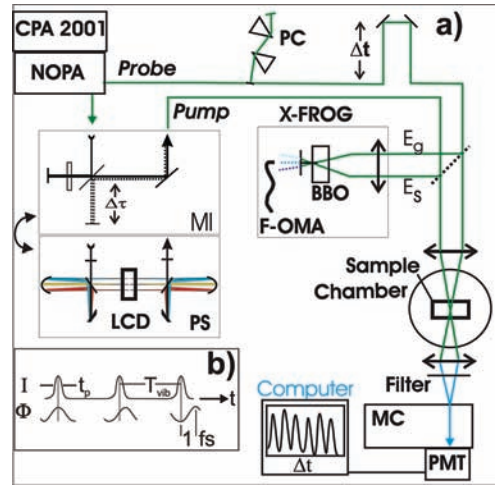

Figure 2. (a) Experimental setup with Ti:Sa laser (CPA 2001), noncollinear optical parametric amplifyer (NOPA), pump and probe beam, prism compressor (PC), pulse shaper (PS), Michelson interferometer (MI), fiber spectrometer (F-OMA), monochromator (MC), photomultiplier tube (PMT), sample chamber, and X-FROG analyzer with gate and signal beams E_g and E_s. (b) Sketch of the pulse train intensity I leaving the shaper setup, with controlled relative phase Φ on the order of 1 fs. The pulse duration t_p indicates the length of 40 fs, the subpulse delay is adjusted to match one vibrational period of T_{vib} = 250 fs.

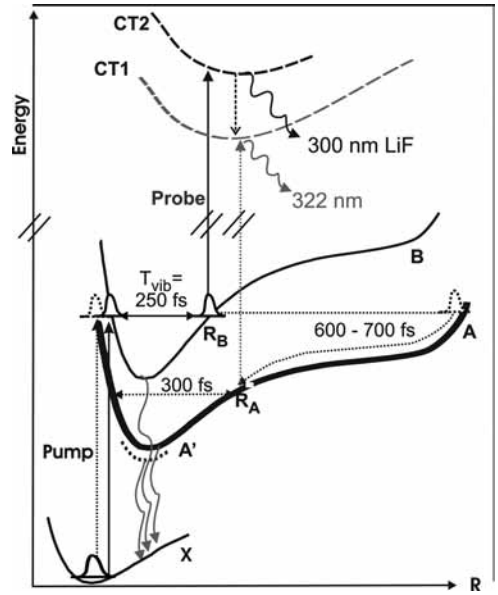

Figure 3. Potential energy scheme with vibrational wave function in electronic ground-state X and wave packet generation (Pump) in covalent states B (solid) and A (dotted), respectively. Wave packets at probe positions R_A and R_B are lifted (Probe) to charge transfer states CT1 and CT2 which fluoresce at 322 and 300 nm, respectively. Wave packet oscillation in B with round trip time T_{vib} is indicated by a solid arrow and the relaxing one in A by a dotted arrow and characteristic times. Wavy arrows from the vibrational ground states of B, A, and A′ indicate fluorescence to the X state.

in Figure 4b the A background is suppressed. Exclusively the B state vibrational progression is obtained with sharp zero phonon lines (ZPL), blue-shifted broad phonon sidebands (PSB), and an accumulation at shorter wavelength of higher order phonons.

Figure 4c displays as a solid line the comb for 40 fs pulses which is generated in the Michelson device if the second pulse delay is tuned to a vibrational round trip (analogue to Figure 1g,h,i) and the phase to a maximal overlap with the ZPL and

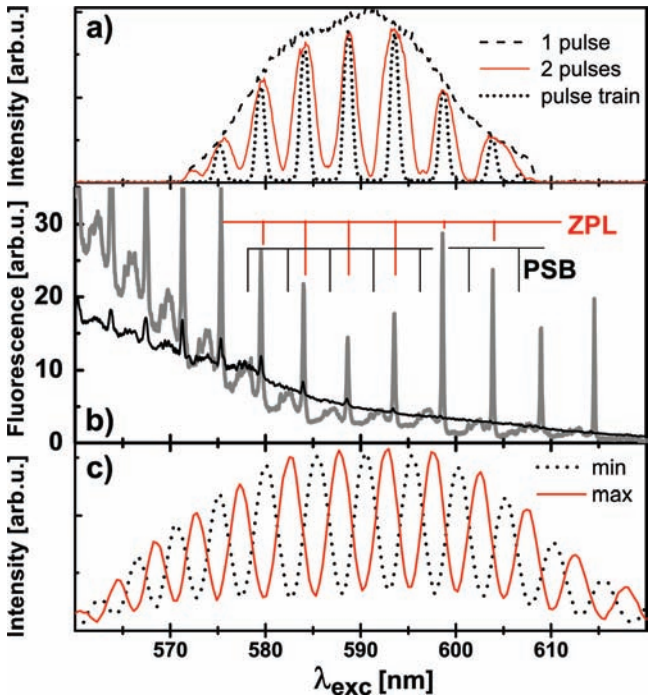

Figure 4. (a) Spectral representation of a single pulse (dashed line), two pulses (solid line), and a pulse train (dotted line) matching the zero phonon lines (ZPL). (b) Excitation spectrum of the B state (thick gray line) and the A′ state (thin black line) with indicated positions of the ZPL and the phonon sidebands (PSB). (c) Broad spectral fringe pattern of the Michelson interferometer experiments. The solid fringes give maximal fluorescence signal; the dashed fringes give a minimal one.

PSB contributions. A maximal overlap catches in one fringe wing the ZPL in the center and in the other wing most of the PSB. The minimal overlap places the maximum of the comb just in the low intensity regions between the blue end of PSB and the next ZPL as shown by the dotted line in Figure 4c. This demonstrates that selection is possible with two pulses, but the spectral resolution is not sufficient to separate ZPL and PSB. The dashed line in Figure 4a shows a spectral envelope now after passing just one pulse through the fully transmitting pulse shaper unit. Programming the ZPL center positions with a sinusoidal amplitude modulation and appropriate phases into the shaper's LCD leads to the two-pulse spectrum in red of Figure 4a. Programming sharper ZPL lines with a period of 3 open ZPL pixels and around 14 closed pixels between the ZPL (matching the B state anharmonicity) leads to the dotted comb with a ZPL contribution now well separated from PSB. This comb can be tuned to ZPL, PSB and also to the low intensity intervals just in front of ZPL, called A position in the following. In this way, well-defined wave packets with the underlying Br_2 vibrations decoupled or coupled to the lattice phonons are prepared. The resulting pulse sequences in time space and their phase distributions will be analyzed in section 4.1.

2.2. Experiment. The setup is shown schematically in Figure 2a. Samples were prepared from a (500:1) gas mixture stored in a glass vessel consisting of Ar gas with 99.9999% purity (Linde) and Br_2 with isotopomers in natural abundance (purity 99.99% Sigma Aldrich). Approximatley 70 μm thick samples were grown in an ultrahigh vacuum chamber within 3 h on a CaF substrate kept by a liquid He flow cryostat at 20 K and cooled to 6 K after deposition. In this way rather clear polycrystalline films were obtained with a minimal inhomogeneous broadening of ZPL according to excitation spectra like in Figure 4b.

Fluorescence from the samples was collected by a $f = 10$ cm fused silica lens and imaged in a $f = 25$ cm monochromator after appropriate filtering. Emission from the A, A′, and B states in the spectral range from 600 to 1100 nm was recorded with a spatially resolving liquid N_2 cooled charge coupled device (OMA 4000 EG&G) covering a range of 125 nm with a resolution of 0.1 nm per pixel line. In the pump−probe scheme sketched in Figure 3, charge transfer states of Br_2 are populated which deliver rather broad band fluorescence centered at 322 and 300 nm.[18] This UV fluorescence is recorded behind the exit slit of the monochromator MC with a photomultiplier PMT and boxcar integrator optimized to the 1 kHz repetition rate. The time delay between pump and probe pulse was scanned typically with a step width of 10 fs, and 4000 pulses were averaged for noise reduction. The fundamental of a commercial Ti:Sa laser (Clark-MXR CPA 2001) at 775 nm with a band width of 8 nm (170 fs pulses of 750 μJ energy) was used to pump a noncollinear optical parametric amplifier (NOPA in Figure 2a). The NOPA is tunable between 460 and 650 nm and delivers typically 40 fs pulse duration with 5−6 μJ per pulse. It was centered at 590 nm and fed after compression in the prism compressor PC into a Michelson interferometer (MI in Figure 2a) or split for the shaper experiment into equally strong beams. One of them, the probe beam in Figure 2a, was compressed, time delayed by Δt in a stepping unit with a step width of 10 fs and superimposed with the second beam, the pump beam, on the sample in an about 50 μm diameter focal spot. The pump beam passed the pulse shaper (PS) where it is converted into a pulse train by spectral programming. Its polarization relative to the probe beam is optionally modified from parallel to perpendicular by a $\lambda/2$ plate.

The spectral profile was measured with a fiber coupled optical multichannel analyzer (F-OMA: Ocean Optics 2000) which served also for the spectral comb calibration in the Michelson interferometer experiment. The timing properties of the pulse sequences were analyzed by frequency-resolved optical gating (FROG) in the X-FROG geometry by cross correlating the pump beam E_s in Figure 2a with the probe beam E_g in a BBO crystal and detecting the phase-matched second harmonic.[19] The single short probe pulse serves as a fast gate to record the time-dependent amplitude and phase (chirp) in the pulse sequence of the pump beam.

In the Michelson interferometer, one beam passes the 50:50 beam splitter once and the other beam three times. The group velocity dispersion in the optical material induces a chirp difference which could be compensated by an additional plate in the first beam. We use such a plate; however, we keep purposely a negative chirp difference of the pulse arriving first on the sample with respect to the second one with a value of $\beta' = -0.3$ fs cm. With β' we compensate[14] the known anharmonicity of Br_2 in Ar in this region of $\omega_e x_e = 1.7$ cm^{-1}. Without this correction, the comb pattern in Figure 4c which includes this effect, would no longer match all the lines in the vibrational progression. The anharmonicity delays the higher v' components compared to the lower ones in the vibrational wave packet prepared by the first pulse. The higher v' are started earlier due to this negative chirp, and after the first round trip they just line up with the second pulse. Thus, the optimal focusing time T_{opt} in a Morse potential given by

$$T_{opt} = \frac{\beta' v^2}{4\pi\omega_e x_e} \quad (1)$$

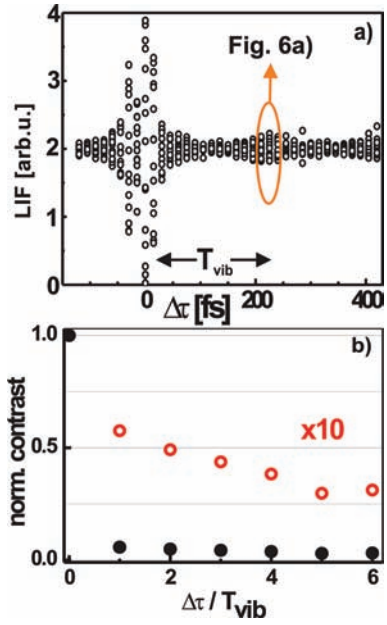

Figure 5. (a) Phase-locked pulse pair (PLPP) experiment with normalized B → X fluorescence signal vs. time delay $\Delta\tau$ between the two Michelson pulses at 590 nm (open circles). Constructive and destructive interferences of the excited wave packets for the 16 different phases lead to maxima and minima of the signal. Phase tuning is shown in Figure 6a. (b) Modulation contrasts of phase-dependent signals taken at different time delays nT_{vib}. The amplitude is normalized to the one at $\Delta\tau = 0$ (solid circles) and magnified by a factor of 10 (open circles).

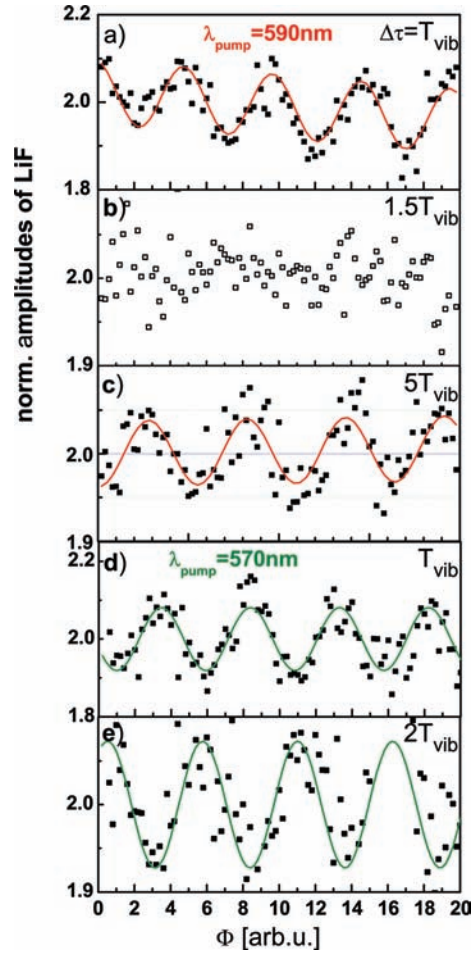

Figure 6. Normalized B → X fluorescence like in Figure 5 vs phase ϕ from piezo tuning with about 64 values distributed over 6π. Taken at a central pump pulse wavelength of (a−c) 590 nm and (d, e) 570 nm. The coarse delay times $\Delta\tau$ for (a) to (e) are 1, 1.5, 5, 1, and 2 times the round trip time T_{vib} = 250 fs for 590 nm and T_{vib} = 270 fs for 570 nm, respectively.

just corresponds to the round trip time T_{vib} = 250 fs for the central ν = 135 cm^{-1}.[20] The coarse scanning of one mirror by a stepping motor to adjust the subpulse separation $\Delta\tau$ for T_{vib} has to be combined with a fine-tuning of the second mirror by a piezo driver in order to scan the phase ϕ of the electric field with subfemtosecond resolution (Figure 2b). The high stability can be achieved either by a demanding feedback loop[21] or by applying the COIN variant[22] that accepts statistical fluctuations, however, loses the phase information. Here we scan for every $\Delta\tau$ a series of 64 ϕ values and record with the F-OMA of Figure 2a the spectral fringes as suggested in ref 23. They allow reading of the absolute value of ϕ in reference to $\phi = 0$ at the ZPL comb, and this ϕ value is then combined with the recorded intensity in Figure 5 and Figure 6.

The pulse shaper is a standard 4-f setup with imaging of the parallel diffracted color beams from the first grating in Littrow configuration by a spherical mirror in normal incidence via a plane deflection mirror in the Fourier plane where the LCD is located. The color separated beams are combined by a mirrored combination of a second grating and mirrors. Gratings with 2000 lines/mm and a focusing length of f = 13 cm are used. The LCD consists of two arrays each with 128 pixels and crossed extraordinary axis by 90°. This allows for amplitude and phase shaping. For the pulse train experiments only amplitude shaping is applied by keeping the phase retardances of the sum of both plates fixed and varying only the differences. The phase voltage calibration was adapted for each pixel, and a contrast of 200:1 was achieved for transmission maximum to minimum. The pixel width is 97 μm with a 3 μm gap. Thus, the whole unit covers a spectral range of 40 nm and each pixel corresponds to 0.3 nm. For single pulse experiments, all pixels were set to full transmission (Figure 4a dashed envelope). Programming of double pulses was started with a sinusoidal pattern and optimization of phase and amplitude to achieve spectral coincidence of the shaped spectrum with the excitation spectrum (Figure 4a, red comb). For the pulse train, the ZPL comb was programmed (Figure 4, dotted comb) as an exact copy of the excitation spectrum and then shifted to PSB and A positions. It leads to seven strong pulses in time frame, as will be shown later on. We want to point out that despite the exclusive amplitude shaping in frequency domain the pulse train acquires the necessary relative phase pattern in time domain, apparent for example from the Michelson double pulse case, and it will be derived later on by Fourier transformation.

3. Results

3.1. Double Pulses from a Michelson Interferometer. Figure 5 shows a measured interferogram by recording the intensity of the B → X fluorescence out of $v' = 0$ vs the time difference $\Delta\tau$ of the two pulses. For each $\Delta\tau$ the relative phase ϕ between the electric fields of the two pulses was varied between 0 and 2π in 16 steps. The intensity for each step is given by the open circles. The pump pulse was centered around 590 nm and covered several vibrational levels around $v' = 9$ of the Br_2 B-state. The first recurrence at $\Delta\tau$ = 250 fs represents one vibrational round trip time in this energetic range.[14,24] It is marked with the ellipse. To investigate the phase dependence in more detail, $\Delta\tau$ was fixed and the relative phase ϕ was varied in small steps covering 8π. Figure 6a displays the obtained

modulation (squares) together with a sine fit (solid line). Each data point is extracted from emission spectra by integrating for the (79, 81) isotopomer the three emission bands B($v' = 0$) → X($v'' = 12, 13, 14$) around 860 nm on the CCD.

This experiment was repeated for several fixed $\Delta\tau$, and a selection is shown in Figure 6. Experimental values are normalized such that the incoherent average value is set to two like in Figure 5a. Plots a−c originate from 590 nm and plots d and e from 570 nm excitation wavelength. The pulse length was 40 fs in both cases. The sinusoidal modulation is maximal for $\Delta\tau = T_{vib}$ in Figure 6a, where the two wave packets meet at the inner turning point and can interfere optimally on the molecule, either constructively (maximum) or destructively (minimum). A significant modulation contrast up to the sixth round trip time $\Delta\tau = 6T_{vib}$ was observed in Figure 5b, however, with decreasing amplitude. For longer time delays the modulation lies within the noise level. Figure 6 shows that this modulation, in (a) for $\Delta\tau = T_{vib}$ and (c) with $\Delta\tau = 5T_{vib}$, is really caused by interference, since no modulation is observed in plot b) for $\Delta\tau = 1.5T_{vib}$. For 1.5 T_{vib}, the two wave packets are localized at the inner and outer turning points, respectively, which inhibits interference in the Franck−Condon region. Irregularities in the modulation period of measured data (squares) are visible by comparison with sine fits (solid lines) and are caused by nonlinearities of the piezo drive, which controls the relative phase ϕ. Finally, emission from A′($v' = 0$) → X($v'' = 11$) is recorded. However, no modulation beyond noise appears. Thus, no interference effects for the A′ contribution are observed (not shown).

Another experiment that covered the spectral region around 570 nm higher up in the potential around $v' = 13$ is shown in parts d and e of Figure 6. Here, the Franck−Condon factors are larger by a factor of 10. The modulation contrast for $\Delta\tau = T_{vib}$ in Figure 6d is comparable to the excitation with 590 nm in (a). Plot e shows clearly the second recurrence of the wave packet. For $\Delta\tau = 5T_{vib}$, no interference could be observed anymore. The earlier loss of observed interferences at 570 nm in comparison to the $\lambda_{pump} = 590$ nm case represents the reduction of spectral contrast for ZPL and PSB in the excitation spectrum in Figure 4b compared to the overwhelming background. Therefore, this region around 570 nm is less favorable for coherent control, and further experiments are performed with pulses centered around 590 nm.

Figure 4c shows the spectral fringes in the interference pattern for $\Delta\tau = 1T_{vib}$ at 590 nm excitation. Those corresponding to maximal LiF signal are plotted as a solid line and those to minimal signal as dashed line. The comparison with the B-state excitation spectrum of Figure 4b demonstrates that the maximal pattern is not centered to the ZPL, as would be expected for a free molecule. For Br_2/Ar it is not possible to position a fringe minimum on a ZPL without exciting a PSB and vice versa. Therefore, the fringe patterns of minimal and maximal LiF signal are situated between ZPL and PSB, since the signal height is determined by the overlap of spectral interferogram and excitation spectrum, as will be discussed in section 4.1.

Before starting with control experiments which require a coherent superposition of a sequence of pulses lasting for more than 1 ps, it is desirable to validate that for the investigated electronic transition electronic coherence prevails on such a long time scale. The line width of the ZPL in ref 14 predicts a lifetime of at least 1 ps at 590 nm. The Michelson test experiments confirm this information and deliver additional information on the efficiency. The modulation contrast of the B-state fluorescence as in Figure 5a is collected in Figure 5b for seven different time delays, $\Delta\tau$. The large drop from $\Delta\tau = 0$ to $\Delta\tau = T_{vib}$ is caused by several contributions. In the case of $\Delta\tau = 0$, an observed optical interference of light with a contrast of 0.9 represents the unbalanced Michelson interferometer quality. This contrast is strongly reduced in the molecule (from $\Delta\tau = T_{vib}$ on and higher) for several reasons. Incoming light is most likely absorbed by the A state, and not by B. The parts absorbed by the A state continuum (Figure 4b) do not contribute to the interference contrast. Furthermore, population that leaves the B state via predissociation[14] to a repulsive state or undergoes energy relaxation does not return to the inner turning point to interfere with the second wave packet. The B-state vibrational progression is detected on the continuum of the A′ fluorescence. Since this B-state fraction on the A′ excitation spectrum is only in the range of 1−2%, a recursion is not apparent in the A′-state′s fluorescence according to the experiment. The contrast strongly depends on the electronic coherence between the two electronic states since interference can only be observed if overall coherence is maintained. From vibrational wave packet revivals and focusing experiments in ref 20, the vibrational coherence time of Br_2 in solid Ar was determined to be 3 ps. The faster decaying modulation contrast in the phase-locked pulse pair (PLPP) spectrum of the B state in Figure 5b indicates, therefore, a loss of electronic coherence in the range of $6T_{vib}$, corresponding to 1.5 ps for Br_2 in an Ar solid. Indeed, we observe two decays, a very fast one from the first to the second round trip time and a slower one, which persists over 1.5 ps. The latter is in accord with the line width of the ZPL which reflects the fastest decay process (1 ps at 590 nm), which usually is the electronic coherence. For Cl_2:Ar the electronic coherence was observed for 660 fs, while the vibrational coherence lasts for more than 3 ps.[25]

3.2. Pulse Train Results. The Michelson experiments investigate the superposition effect of phase stable wave packets on excitation, i.e., essentially absorption spectra. A separation of ZPL and PSB contributions is not obvious as illustrated by the position of the maxima and minima of the combs in Figure 4c. Therefore, the pulse train experiments are based on a more informative pump−probe scheme sketched in Figure 3. From previous experiments we know that wave packets in the B and A states can be lifted in a two photonic process to two tiers of charger transfer states form where they emit either at 322 nm (CT1) or at 300 nm (CT2).[24] The spatial probe window positions R_A and R_B should be located just at the outer turning point for 590 nm pump and probe. Excitation to CT2 should lead to 300 nm emission and by nonradiative relaxation also to 322 nm emission. R_A is located deeper in energy, and therefore only CT1 can be reached.

This scenario is first confirmed in Figure 7a for 322 nm fluorescence by a single pump pulse and probe pulse experiment both at 590 nm as in all following measurements. The first two pronounced peaks are marked by A1 and A2 since they originate from a wave packet in the A state. The A state wave packet is prepared at the inner limb and propagates with high kinetic energy toward the outer limb. On this way it passes R_A for the first time at around 100 fs delay, giving rise to the first peak A1. It is sharp due to the high velocity causing a short time in which R_A is crossed. It is strong, indicating a large population in A combined with a good detetion efficiency. In the gas phase it would be above the dissociation limit and not return. In the matrix it is caged and scattered back by the surrounding matrix atoms at R values around 3.6 Å. This process has been studied in detail near the B state dissociation limit.[24] The scattering is very inelastic; most of the kinetic energy is lost. After a time

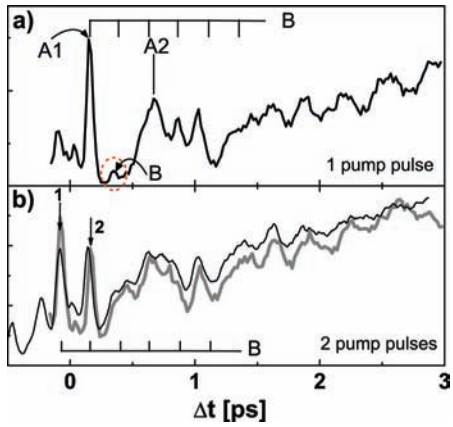

Figure 7. Comparison of single pump and double pump−probe spectra at $\lambda_{fl} = 322$ nm from CT1. (a) Single pump−probe spectrum (solid line) with first and second passage of R_A at A1 and A2. The B vibrational period is indicated by ticks. The second passage of R_B is marked by the dashed ellipse. (b) Reconstruction of double pump−probe spectrum (thick gray line) by adding (a) and its copy shifted by T_{vib} of B. Arrows 1 and 2 indicate the two positions of A1. The measured spectrum with double pulse excitation, reconstructed this way, is shown as the thin black line. Details are explained in the text.

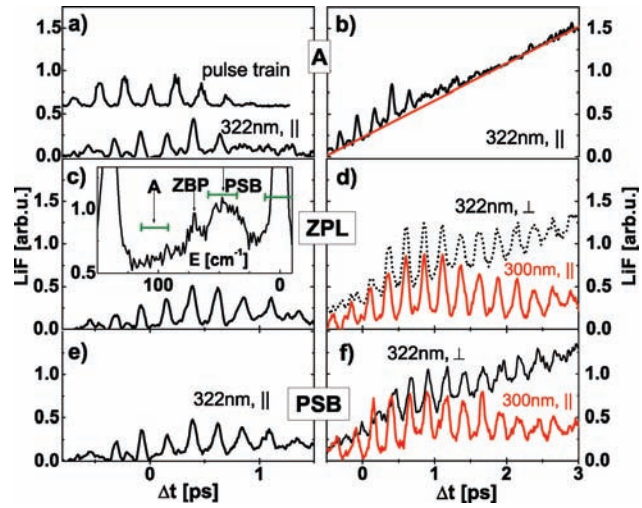

Figure 8. Pump−probe spectra recorded at 322 and 300 nm fluorescence using a pulse train for excitation with a cross correlation shown in (a) (top). (a) (bottom) A comb excitation with 322 nm fluorescence detection in parallel pump−probe configuration derived from (b) after substraction of the indicated linear background (red). (c and e) Analogous for ZPL and PSB comb. (d and f) Compare 322 nm vertical configuration fluorescence and 300 nm parallel configuration without background substraction. Inset in (c) displays the A, PSB, and ZPL segments chosen for the three rows on one phonon sideband and the zone boundary phonon ZBP. The spectra are normalized for better visibility. The PSB spectrum (300 nm) is multiplied by 2 with respect to the ZPL (300 nm) spectrum.

delay of several hundred femtoseconds, the wave packet returns slowly, much deeper on the A state surface as sketched in Figure 3. The second passage of R_A on the return trip is seen in the still strong but late and broad peak A2 in Figure 7a. After this first hard collision, the A wave packet oscillates with a period of 300 fs and with small energy losses, thus approaching from top the resonance energy at R_A. This enhances somewhat the detection efficiency and gives rise to the slowly increasing background beyond 1 ps with weak modulation.[26]

Simulataneously, the B state wave packet is excited at the inner limb. We know from Figure 5 that it oscillates with a period of 250 fs and it should be seen once per round trip at R_B. It relaxes very slowly according to the long coherence in Figure 5b since its excursions deep in the potential well are small. Indeed, a progression of five recurrences can be identified in Figure 7a as indicated by B. Oscillations 1 and 3 coincide with A1 and A2 and are hardly visible in these strong A peaks. The second one is marked with B. The weakness of the B amplitude compared to A is consistent with the small B contribution in Figure 4b and small amplitude at T_{vib} in Figure 5.

Thus, the challenge is obvious: Is it possible with the pulse trains to amplify B with respect to A so that a detailed B investigation is feasible? We start in a systematic way with the double pulse from the pulse shaper to display the trend. The sinusoidal modulation with the ZPL progression is programmed as described in section 2.2 and delivers a phase-stable double pulse in time with the time delay of $T_{vib} = 250$ fs. The spectrum in Figure 7b taken for otherwise comparable conditions as in Figure 7a seems to be even more complex. The first two strong pulses 1 and 2 are just replicas of A1 separated by T_{vib} due to the double pulse excitation. A2 has merged to a very broad structure since T_{vib} does not match with its time delay. The B or T_{vib} period shown by ticks matches with peaks in the spectrum, but the complexity would put question marks on such an assignment. Nevertheless, this trace is fully consistent with Figure 7a and a double pulse excitation. If we repeat Figure 7a with a shift by T_{vib} and add these two spectra, we end up with the gray line spectrum in Figure 7b. It contains all features of the measured double pulse spectrum within the reproducibility of these two independent measurements. There is some progress toward our aim. The A state structures have somewhat lower amplitudes compared to B and have a trend to wash out after the first recursion due to the timing mismatch, but the progress seems not to be convincing.

Next, we switch from the sinusoidal comb (solid red in Figure 4a) to the spectrally sharper comb of Figure 4a (dotted). To illustrate in more detail the relation of the comb to the phonon band structure, we zoom in for one tooth of the comb into the different programmed positions in the insert of Figure 8c. The spectral interval of 130 cm^{-1} between the cut ZPLs of $v' = 8$ and $v' = 9$ is displayed and the PSB extends from the ZPL at 0 up to the peak[27] originating from the zone boundary phonon (ZBP) at 70 cm^{-1}. Three pixels corresponding to windows of 30 cm^{-1} shown in Figure 8c are opened for transmission, as indicated by green bars. They are positioned at A, PSB, and ZPL with the period of the excitation spectrum (Figure 2b) and within the full envelope shown in Figure 4a. With the F-OMA in Figure 2, we record the fringe pattern and check that it coincides with the attempted comb position relative to the excitation spectrum. Now we use the X-FROG and determine the intensity and phase distribution in the resulting pulse train. All three combs (A, PSB, and ZPL) have the same intensity pattern which is reproduced in Figure 8a (top). It consists of seven dominant pulses separated by the B state vibrational period. The combs differ however by the chirp within each pulse which will be discussed in section 4.2.

First, we apply the A comb which lies concerning B in the empty region between the termination of the PSB and the next ZPL. There, we catch the full A background according to Figure 4b. For this case a smooth background, linearly increasing with time, shows up in Figure 8b (red line). On top of it an oscillatory structure is visible which seems similar to the pulse train itself. Indeed, after substraction of the red line we obtain a pattern (Figure 8a) which is identical within noise with the excitation pulse sequence. No oscillations occur anymore after termination

of the pulse. It is just slightly shifted in time due to the propagation to the probe window R_A. Evidently, each subpulse generates an A wave packet with an amplitude proportional to the intensity. Each wave packet is seen once as a peak when it passes R_A for the first time and all further recursions are relaxed and accumulate to the continuously rising structureless background. This behavior is consistent with Figure 7b and shows that only the A1 feature survived with the pulse train. All further A2 and later contributions merge to the background which rises by the addition of pulses together with the improved detection efficiency. Next, the ZPL comb is employed. A similar background is observed. When it is substracted in the same way, an oscillatory structure is observed (Figure 8c) which differs from Figure 8a significantly. The peak intensity grows continuously with the number of pulses until termination of the train. Thus, a clear accumulation occurs which does not reproduce the intensity drops in the train. The modulation proceeds with the same period and initially full amplitude after termination of the train. For the PSB comb (Figure 8e), we obtain qualitatively the same behavior as for ZPL. Obviously for the ZPL and PSB combs the oscillatory structure corresponds nearly exclusively to a B state wave packet which accumulates by constructive interference within the pulse sequence.

We dwell on the ZPL and PSB combs in more detail in parts d and f of Figure 8. In addition, we change the fluorescence detection from 322 to 300 nm and thus suppress already in the recording the relaxed A state background as mentioned before. Now we obtain for ZPL and PSB high-quality spectra (solid lines) which reflect the coherent preparation of B state wave packets and their dynamics after pulse termination for in total 14 periods. PSB dynamics is very similar to that of ZPL. The intensity is reduced by about a factor of 2. A further confirmation of these results is obtained from 322 nm spectra in vertical polarization which are also included in parts d and f of Figure 8). By switching from parallel to vertical relative polarization of pump and probe, the B contributions are enhanced in 322 nm detection. The reason will be treated in a forthcoming paper dealing with predissociation. The 300 nm ZPL spectrum is repeated in Figure 11a to illustrate the nonlinear accumulation in Figure 11b and to compare it with simulations in Figure 11c. Already this qualitative comparison demonstrates that the goal of separating A and B contributions and enhancing B to an extent that ZPL and PSB can be addressed individually has been fully reached with the pulse train.

4. Discussion

4.1. Michelson Results. The drop in contrast for $\Delta\tau > 0$ in Figure 5 and the variation in contrast with recording B or A′ fluorescence is an important aspect which will be discussed by simulations. A calculation for a noninteracting free molecule is demonstrated in ref 21. Here, we have a more complex situation of molecular and phonon degrees of freedom. In such a case interferogramms $I(\Delta\tau, \phi)$ were successfully reproduced[23] by a multiplication of the spectrum of fringes $F_\lambda(\Delta\tau, \phi)$ which varies with $\Delta\tau$ and ϕ with the absorption spectrum $A(\lambda)$

$$I(\Delta\tau, \phi) = \sum_\lambda F_\lambda(\Delta\tau, \phi)A(\lambda) \qquad (2)$$

For F_λ we use calculated fringe spectra and thus we obtain an upper limit of the contrast achievable in the real experiment. F_λ was derived from a Fourier transformation of two pulses centered at 590 nm with a width of 40 nm and a chirp difference

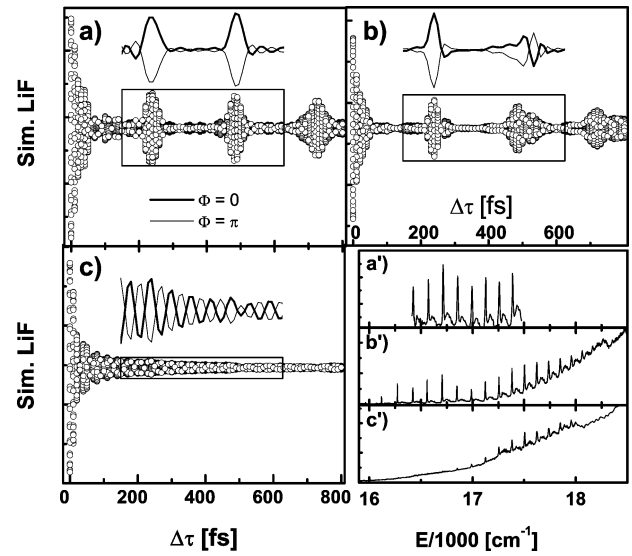

Figure 9. Simulation of a Scherer-type experiment by multiplication of simulated spectral fringes and Br_2/Ar excitation spectra according to eq 2. The simulation applying the cut out of the B excitation spectrum of (a′) is shown in (a) for 32 different phases (open circles) covering 2π. Two special phases in the range of the box are highlighted on top of each data set: $\Phi = 0$ giving maximal (thick line) and $\Phi = \pi$ minimal (thin line) signal at $\Delta\tau = 0$. Analogously, (b) contains the simulation for the full B excitation spectrum, plotted in (b′) and in (c) the A′ excitation spectrum of (c′) was used. Simulation parameters were central wavelength $\lambda_0 = 590$ nm, spectral width $\Delta\lambda = 40$ nm, and chirp parameter $\beta' = -0.3$ fs cm.

of $\beta' = -0.3$ fs cm. $A(\lambda)$ is replaced by the two excitation spectra of Figure 4b and artificial ones in order to understand the influence of selection of fluorescence. In Figure 9 the results for 32 ϕ values for each $\Delta\tau$ are shown. The values for $\phi = 0$ and π are connected by thick or thin lines on top of the inset to increase visibility. An artificial $A(\lambda)$ spectrum is used in Figure 9a which is displayed in Figure 9a′. The continuous background in Figure 4b has been removed completely, and it consists only of the ZPL and PSB structured contributions. A very regular beat pattern spaced by T_{vib} is obtained and $\phi = 0$ follows the maximal envelope and $\phi = \pi$ the minimal envelope, respectively. The contrast at T_{vib} compared to $\Delta\tau = 0$ of 35% exceeds that in the experiment in Figure 5 of 10% considerably, which is not surprising due to the eliminated background. The question arises why it is not closer to unity in the simulation. For this purpose we simulated interferograms for only the ZPL or the PSB contributions of Figure 9a′. The result (not shown here, see ref 28) is that the maximal and minimal envelopes have the same $\Delta\tau$ dependence as in Figure 9a; they are however of opposite phase to each other. Thus, they cancel each other to a large extent and only the difference survives according to the summation in eq 2. Qualitatively this is clear because PSB extends to the center between two ZPL ($\phi = 0$) (Figure 8c) where the fringe is located for $\phi = \pi$. This is also the analytical explanation why the maximal fringe in Figure 4c is off the ZPL position. For Figure 9c we use the other extreme for $A(\lambda)$, namely, the A′ excitation spectrum (Figure 4b and Figure 9c′) with the large A continuous background. The simulation delivers a quick drop and a continuously decaying signal with no resolvable beat structure at T_{vib} or multiples of T_{vib}. This is in full accordance with the not shown experiment. The unstructured amplitude in Figure 9c of 5% from that at $\Delta\tau = 0$ corresponds to the modulation in Figure 9c′ and is about the noise level in the experiment. The B fluorescence excitation spectrum (Figure 9b′) is taken for $A(\lambda)$ in the simulation of Figure 9b, and now

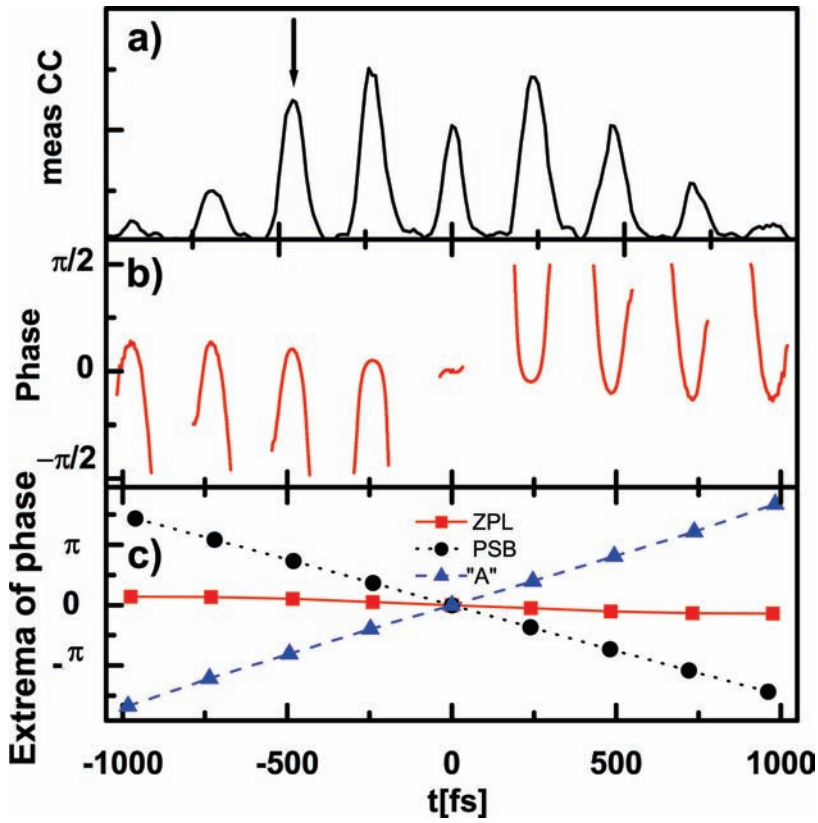

Figure 10. Reconstruction of phases from Fourier transformation of measured frequency resolved spectra. (a) Experimental cross correlation of the pulse train (see Figure 8a and for arrow Figure 11). (b) Plot of the relevant phase information calculated for ZPL position. The phases show a quadratic dependence, corresponding to a linear chirp with changing sign around time zero. (c) Unwrapped extrema values from (b) and for PSB and A positions (phases not shown).

good correlation with Figure 5a could be expected. Qualitatively the beat patterns agree, the contrast in the simulation of 25% exceeds that of 10% in the experiment still significantly. A part of it can be attributed to deficiencies in the experiment. We suspect that also a systematic problem comes into play. We prepare the first wave packet at $\Delta\tau = 0$, the A content is lost by decoherence and the B part returns at $\Delta\tau = T_{vib}$ to the Franck−Condon region. The wave packet from the second pulse consists of a pure B content, which we treat in the simulation, and the pure A content, which will be lost once more due to decoherence. If however also a cross term of B and A forms, which will be incoherent due to its A content, then it is ignored in the simulation of Figure 9b with only B excitation features. In this case, the coherent B part would gain too much weight compared to the experiment.

The envelopes with $\phi = 0$ and π, respectively, shown for second and third T_{vib} in Figure 9 do no longer follow the maximal and minimal contours systematically. For nT_{vib} the fringe spacing is reduced to $1/n$ of the vibrational spacing and the subfringes can coincide with specific structures in the PSB of Figure 8c. Thus, a better separation of PSB and ZPL can become feasible and was exploited in ref 23. In summary, the Michelson experiment is an excellent tool to characterize qualitatively the coherent versus incoherent parts. It can be used to prove with high sensitivity remaining coherence by tuning the phase as shown in Figure 6. The phase-stabilized or fringe-stabilized version used here is required because in COIN a separation from instrumental noise would be questionable. For an analysis of different spectral contents, the Michelson setup is less valuable due to the counteracting contributions. A reconstruction from known $A(\lambda)$ is possible. However, an investigation of not yet resolved contributions would be rather ambiguous.

4.2. Pulse Train and Phonon Coherences. Positioning the spectral combs in Figure 4c via tuning just the phase between two pulses like in Figure 6 is obvious in the Michelson interferometer case. The intensity distribution in the pulse trains of Figure 8a is identical for the A, PSB, and ZPL comb locations. The difference has once more to be contained in the relative phase, despite the fact that only amplitudes were shaped in the LCD of Figure 2. The experience of the interferometer demonstrates that the spectral fringe patterns highlight the temporal phase information in the best way and therefore they are exploited also for the pulse trains to retrieve the phase relations. The fringes were recorded with a F-OMA and Fourier transformed from frequency domain into time domain for the three chosen comb positions. The measured cross correlation in time domain from Figure 8a is repeated in Figure 10a and compared with the phase information within the subpulses obtained from the Fourier transformation. The central peak in frequency domain for ZPL was taken as a reference phase with $\phi = 0$, and the further phases for this fringe are reproduced in Figure 10b. The early peaks (at negative times) have a quadratic phase with negative curvature which corresponds to a negative linear chirp. For peaks at positive times, the sign is switched to positive and this coincides with the expectation for a pulse train, where the chirp of subsequent pulses should compensate for the molecular anharmonicity. An experimental X-FROG trace (not shown, see ref 28) confirms this change in sign and the trend of an increasing positive chirp with positive times away from the center. The unwrapped phase values for the position

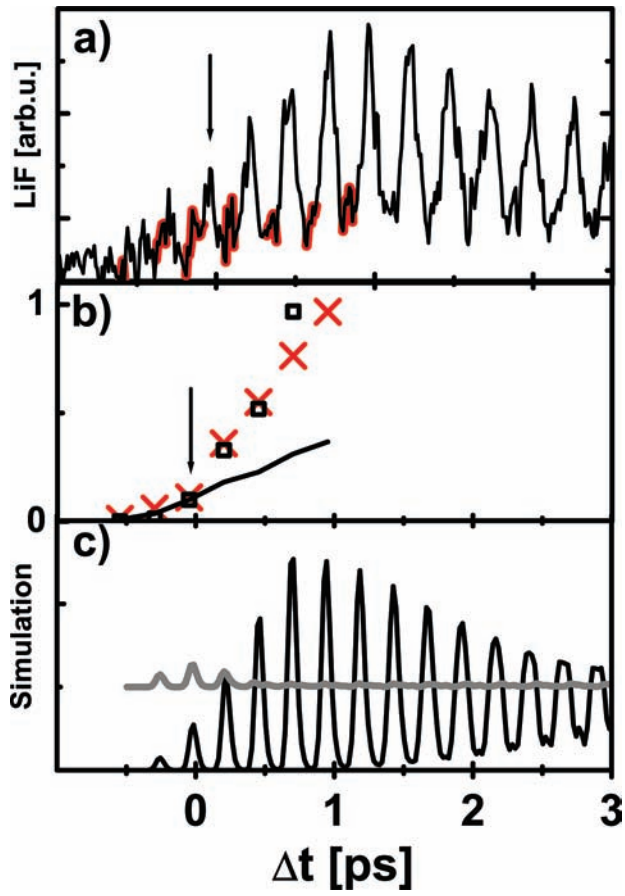

Figure 11. (a) Fluorescence from the 300 nm band showing pronounced B vibrational dynamics and a weak A contribution marked red between the strong B peaks (see Figure 8d). (b) Integrated LiF area from solid line in (a) (crosses), integrated peak intensity from Figure 10a (solid line), and squared integrated peak intensity (open squares). All data are normalized to the peak marked with the arrow (see also Figure 10a). (c) Simulation of the free molecule for constructive (black) and destructive (gray with offset) B excitation (see text).

of the maxima at negative times and minima at positive times are displayed in Figure 10c for the three spectral comb positions. All these phase values follow a linear trend and cross at zero. For ZPL (squares) a horizontal line is observed, as expected, since it is the center of reference. By changing the relative phase between subsequent pulses, the spectral comb can be shifted relative to the envelope, and this was done for the PSB (circles) and for the A excitation (triangles). In both cases the extrema lie on a straight line covering 3π. They are tilted with opposite sign, since the comb was shifted from ZPL position to higher energies for PSB excitation and to lower energies for the position A. Thus, this method of phase reconstruction fully reproduces the expectation from the phase shift picture of spectral combs.

The crucial question is now to which extent these phases are conserved in the accumulation of molecular wave packets. The population P_3^c for three pulses for example with electric fields E_1 to E_3 scales for constructive interference, i.e., $\phi = 0$ with

$$P_3^c(\phi = 0) \sim E_1^2+E_2^2+E_3^2 + 2(E_1E_2+E_1E_3+E_2E_3) \quad (3)$$

The first three terms P_3^{inc} are insensitive to the phase and are present in the coherent and incoherent case. The term in parentheses would be canceled in the incoherent case with statistical phases. It changes sign for coherence with $\phi = \pi$. In the case of pulses with equal field amplitudes E, it compensates the first one and leads to $P_3^c(\phi = \pi) = 0$. Thus, in general the population $P_n^c(\phi = 0)$ for constructive interference of n pulses with equal field amplitude E will scale with

$$P_n^c(\phi = 0) \sim n^2E^2 \quad (4)$$

and the ratio to the incoherent statistical part is given by

$$\frac{P_n^c(\phi = 0)}{P_n^{inc}} = n \quad (5)$$

The ZPL spectrum for 300 nm fluorescence from Figure 8d is repeated in Figure 11a. The increase of integrated intensity from peak to peak in this spectrum is shown by the crosses in Figure 11b. For the duration of the underlying pulse train in Figure 10a the integrated intensity in the subpulses themselves follows the solid line in Figure 11b which is normalized to the crosses for the first strong peak indicated by the arrow in Figure 10a. The stronger than linear increase with the number of pulses is evident. The train consists of five pulses with comparable intensity, and if we square the intensity in the solid line, we obtain the square dots in Figure 11b. Thus, the ZPL contribution of the B state signal accumulation preserves coherence for the overall duration of the pulse train of 1 to 1.5 ps. This holds however only for the B state contribution. The A state continuum lies below the ZPL (Figure 4b), and an A state contribution should be present also in the ZPL comb excitation. Indeed, there is a weak red-shaded contribution in Figure 11a which can be identified with the A part. For the first pulses up to the arrow it is comparable in amplitude to the B part. For later pulses the B part rockets upward according to the square dependence of eq 4, while the A part stays at low amplitude. This illustrates in a direct comparison the coherent accumulation of B and the incoherent one of A. The A part represents a linear replica of the intensity pattern of Figure 10a, like that observed for the A comb in Figure 8a due to energy relaxation and mismatch in timing.

To simulate the coherent B dynamics for constructive and destructive interference for pulse trains (black and gray lines in Figure 11c, respectively), we adapted a published code[20,29] which treats excitation of wave packets in first-order perturbation theory and their quantum mechanical propagation. We include experimental X- and B-state parameters and appropriate probe window conditions, but no depopulation and decoherence.[14] The black line in Figure 11c shows the simulated result for the ZPL configuration, and the agreement with experiment in Figure 11a is very convincing.

Finally, we treat the 300 nm LiF for the programmed PSB comb (Figure 4b) as depicted in Figure 8f as red line. We observe once more a progressive increase in the beginning. The intensity stays however constant after the center of the pulse sequence, and the final signal is lower by a factor of 2 to 2.5 compared to Figure 8d, which is explained now. After coherent superposition of the full pulse train the spectral sharpness of the frequency comb covers the full ZPL and even the most stringent interference of the last pulses do not cut into it (Figure 4a). This is different for the broad PSB. Thus, the destructive part of the interference conditions cuts more and more of the PSB and the progressive constructive part has to compensate for this loss. The spectral weight of the PSB included within the chosen bandwidth of 30 cm^{-1} is about half of that of the

ZPL. If we multiply the plot of Figure 8f with these weight factors, we come close to the coherent result in Figure 8d. This consideration shows the lasting coherence properties of the PSB.

To emphasize the coherence even throughout the whole PSB, we turn back to excitation in the A position in Figure 8a (bottom). The power spectra for all three excitation positions ZPL, PSB, and A (Figure 8a top) are identical, and only the phases determine the selection of the favored comb position by interference. Every pulse with its 40 fs duration covers the full spectrum (Figure 4a), and in an incoherent accumulation with statistical phase, we would observe B wave packets linearly increasing with deposited intensity. The long lasting vibrational coherence in B would preserve this contribution also at long times. There is however no discernible B contribution in Figure 8a, and this can only be explained by a destructive interference of new wave packets with the former ones in B. The destructive interference with the full phonon contribution (ZPL and PSB) requires that also PSB wave packets preserve the phase memory for several round trips. The gray line in Figure 11c shows the result of the simulation for the pulse sequence at comb position A. An offset is added for better visibility. The first pulses generate some population in B. However, the more pulses that are added, the more efficiently population is depleted because destructive interference becomes more stringent. At the termination of the pulse train no discernible population survives, in full agreement with the experiment in Figure 8a. This emphasizes the high phase stability for ZPL and PSB wave packets. For ZPL it is consistent with the narrow spectral width yielding a lifetime of 1.5 ps while a conversion of the full PSB would only correspond to about 100 fs. Obviously, the PSB represents a distribution of phonon modes with long living individual components. Phonons originate from an expanding electronic wave function in the B → X transition (displacive excitation of coherent phonons, DECP) and also the intramolecular vibrations couple to the matrix, according to the spectroscopic evidence.[27] The PSB shape resembles the Ar phonon density of states[14] and the maximum around 70 cm^{-1} in the inset of Figure 8c can be attributed to the zone boundary phonon (ZBP).[30] Scrambling within the phonon modes and even only a propagation of the phonon part in the excitation from the chromophore into the surrounding bulk changes the transition energy and thus the very sensitive electronic coherence. Coherent ZBP coupled for several picoseconds to the chromophore were observed in the DECP process, and the weak damping was attributed to its vanishing group velocity.[30] For the PSB comb (Figure 4a) we cut out a 30 cm^{-1} broad band in the middle part around 40 cm^{-1} shown in Figure 8c. It is remarkable that electronic and vibrational coherence extend into the picosecond regime also for all those modes being resonant with delocalized matrix phonons. For this range of the phonon dispersion curve the sound velocity is 10−15 Å/ps. The phonon amplitudes should spread out in 1 ps over several shells of neighboring atoms as predicted also by classical trajectory calculations.[31] The extinction of B-state contributions in Figure 8a by destructive interference for excitation in the A comb situation indicates however that the major part of the phonon modes preserves electronic coherence during the full pulse sequence. This lasting coherence in a rather large volume containing several hundred atoms calls for an extension of the existing path integral[32] and quantum calculations[33] to catch the essence of these challenging coherence effects. They provide the prerequisite for the proposed coherent control of the matrix induced and phonon supported predissociation.[12]

5. Concluding Remarks

A Michelson interferometer and a programmable pulse shaper unit have been applied in order to select, amplify, and steer a tiny coherent vibronic content in a dominant background provided by an incoherent coupling to the crystalline bath. The interferometer device delivers a sensitive and unambiguous signature for lasting electronic and vibrational coherence in response to active phase tuning since it rests on a coherent superposition of wave packets in a vibronic transition. The spectral resolution in the underlying frequency comb is low, the anharmonicity compensation is less flexible, and a derivation of more subtile features is difficult due to partially compensating contributions. Programming the spectroscopic fingerprint of a vibronic progression in the LCD placed in the Fourier plane of the shaper unit delivers automatically its Fourier transformation into time domain on the sample. The resulting pulse train carries all the characteristic amplitude and phase information in its electric field as has been demonstrated. Recording of the spectral fringes in a spectrometer provides the absolute phases with respect to the carrier envelope. They are required in the interferometer case and allow for a convenient check of performance and stability in the shaper case. The intensity of each subpulse in the pulse train generated by the shaper is reduced with increasing spectral resolution due to the decrease in shaper transmission and the splitting into several subpulses. The individual subpulse intensity decreases in our example by about a factor of 20 in the case of ultimately applied resolution. The broad band and incoherent contribution of the A state, where only the first passage remains resolved, is reduced in the pump (pulse train)−probe spectra accordingly. The selected B state ZPL progression with its small line width is not affected, and it profits from the nonlinear coherent accumulation. The combination of both effects leads to the apparently increasing dominance of the B state contribution with rising resolution and longer pulse sequences as compared to the A state. Thus, this spectral programming represents a very intuitive, straightforward and efficient way to amplify buried coherent contributions, provided that some spectroscopic information is available or it can be guessed and tested in this way. The lasting coherence of the ZPL vibronic progression is in agreement with the small line width. A similar long term coherence in the broad PSB is evident from the experiment. It is required for an experimental realization of the theoretically predicted coherent control of phonon induced predissociation which can now be tackled. The vibronic coherence in the PSB implies electronic coherence including the coupled motion of several hundred Ar matrix atoms in the vicinity of the Br_2 chromophore. This remarkable coherence calls for a theoretical analysis which can clarify if it has to be attributed to a special property of the Ar matrix or if it is of more general nature.

Acknowledgment. We thank Dr. M. Gühr, Dr. A. Borowski, Professor O. Kühn, Professor J. Manz, and Professor B. Gerber for intense discussions and the DFG with SFB 450 for financial support.

References and Notes

(1) Katsuki, H.; Hosaka, K.; Chiba, H.; Ohmori, K. *Phys. Rev. A* **2007**, *76*, 013403.
(2) Nuernberger, P.; Vogt, G.; Brixner, T.; Gerber, G. *Phys. Chem. Chem. Phys.* **2007**, *9*, 2470–2497.
(3) Hauer, J.; Buckup, T.; Motzkus, M. *J. Chem. Phys.* **2006**, *125*, 061101.
(4) Heller, E. J. *Acc. Chem. Res.* **1981**, *14*, 368.
(5) Heller, E. J.; Tomsovic, S. *Phys. Today* **1993**, *46*, 38.

(6) Alimi, R.; Gerber, R. B.; Apkarian, V. A. *J. Chem. Phys.* **1990**, *92*, 3551–3558.
(7) Apkarian, V. A.; Schwentner, N. *Chem. Rev.* **1999**, *99*, 1481–1514.
(8) Bargheer, M.; Borowski, A.; Cohen, A.; Fushitani, M.; Gerber, R.; Gühr, M.; Hamm, P.; Ibrahim, H.; Kiljunen, T.; Korolkov, M.; Kühn, O.; Manz, J.; Schmidt, B.; Schröder, M.; Schwentner, N. Coherence and control of molecular dynamics in rare gas matrices. In *Analysis and Control of Ultrafast Photoinduced Reactions*; Kühn, O., Wöste, L., Eds.; Springer Series in Chemical Physics 87; Springer: Berlin, 2007.
(9) Bargheer, M.; Cohen, A.; Gerber, R. B.; Gühr, M.; Korolkov, M. V.; Manz, J.; Niv, M. Y.; Schröder, M.; Schwentner, N. *J. Phys. Chem. A* **2007**, *111*, 9573–9585.
(10) Gerber, R. B. *Annu. Rev. Phys. Chem.* **2004**, *55*, 55–78.
(11) Sheng, L.; Gerber, R. B. *J. Chem. Phys. (Commun.)* **2007**, *126*, 21108–21110.
(12) Borowski, A.; Kühn, O. *Chem. Phys.* **2007**, *117*, 521–533.
(13) Bondybey, V. E.; Bearder, S. S.; Fletcher, C. *J. Chem. Phys.* **1976**, *64*, 5243–5246.
(14) Ibrahim, H.; Gühr, M.; Schwentner, N. *J. Chem. Phys.* **2008**, *128*, 064504.
(15) Borowski, A.; Kühn, O. *Theor. Chem. Acc.* **2007**, *117*, 521–533.
(16) Tannor, D. J. *Introduction to Quantum Mechanics, A Time-Dependent Perspective*; University Science Books: Sausalito, CA, 2007.
(17) Brandenhorst, M. P. A.; Londero, P.; Wasylczyk, P.; Brif, C.; Kosut, R. L.; Rabitz, H.; Walmsley, I. A. *Science* **2008**, *320*, 638–643.
(18) Gühr, M. *Coherent Dynamics of Small Molecules in Rare Gas Crystals*; Cuvillier Verlag: Göttingen, 2005.
(19) Linden, S.; Giessen, H.; Kuhl, J. *Phys. Status Solidi B* **1998**, *206*, 119.
(20) Gühr, M.; Ibrahim, H.; Schwentner, N. *Phys. Chem. Chem. Phys.* **2004**, *6*, 5353–5361.
(21) Scherer, N. F.; Matro, A.; Ziegler, L. D.; Du, M.; Carlson, R. J.; Cina, J. A.; Fleming, G. R. *J. Chem. Phys.* **1992**, *96*, 4180–4194.
(22) Kinrot, O.; Averbukh, I. S.; Prior, Y. *Phys. Rev. Lett.* **1995**, *75*, 3822–3825.
(23) Fushitani, M.; Bargheer, M.; Gühr, M.; Ibrahim, H.; Schwentner, N. *J. Phys. B: At., Mol. Opt. Phys.* **2008**, *41*, 074013.
(24) Gühr, M.; Schwentner, N. *J. Chem. Phys.* **2005**, *123*, 244506.
(25) Fushitani, M.; Bargheer, M.; Gühr, M.; Schwentner, N. *Phys. Chem. Chem. Phys.* **2005**, *7*, 3143–3149.
(26) Gühr, M.; Bargheer, M.; Fushitani, M.; Kiljunen, T.; Schwentner, N. *Phys. Chem. Chem. Phys.* **2007**, *9*, 779–801.
(27) Gühr, M.; Bargheer, M.; Schwentner, N. *Phys. Rev. Lett.* **2003**, *91*, 085504.
(28) Ibrahim, H. *Tracking coherences in a dissipative ocean: Analysing and controlling Br_2/Ar matrix*; Cuvillier Verlag: Göttingen, 2008.
(29) Tannor, D.http://www.weizmann.ac.il/chemphys/tannor/home.html.
(30) Gühr, M.; Schwentner, N. *Phys. Chem. Chem. Phys.* **2005**, *6*, 760–767.
(31) Kiljunen, T.; Bargheer, M.; Gühr, M.; Schwentner, N. *Phys. Chem. Chem. Phys.* **2004**, *6*, 2185–2197.
(32) Ovchinnikov, M.; Apkarian, V. A. *J. Chem. Phys.* **1998**, *108*, 2277–2284.
(33) Borowski, A.; Kühn, O. *J. Photochem. Photobiol., A* **2007**, *190*, 169–176.

JP900287M